How phage L capsid decoration protein distinguishes between nearly identical binding sites on an icosahedral virion

Rebecca Newcomer [1], Jason R. Schrad [2], Eddie B. Gilcrease [3], Sherwood R. Casjens [3], Michael Feig [2], Carolyn M. Teschke [1], Andrei Alexandrescu [1], and Kristin N. Parent [*2]

Affiliations

[1] University of Connecticut, Department of Molecular and Cell Biology, Storrs, CT 06269; USA

[2] Michigan State University, Department of Biochemistry and Molecular Biology, East Lansing MI, 48824; USA

[3] University of Utah School of Medicine, Division of Microbiology and Immunology, Department of Pathology, Salt Lake City, 84112; USA

Running title: Structural biology of capsid binding by Dec

* To whom correspondence should be addressed

Kristin N. Parent

Dept. of Biochemistry & Molecular Biology

Michigan State University

603 Wilson Rd

519 Biochemistry Building

East Lansing MI, 48824

Key Words: bacteriophage, cryo-electron microscopy, cementing protein, capsid assembly, computational modeling, NMR

Abbreviations: cryo-EM; cryo-electron microscopy, 3DR; three-dimensional reconstruction, MD; molecular dynamics, NMR; nuclear magnetic resonance.

Abstract

The major coat proteins of most dsDNA tailed phages and viruses form capsids by a mechanism that includes active packaging of the dsDNA genome into a precursor procapsid, and subsequent expansion/stabilization of the capsid. Packaging of dsDNA genomes accrues ~10 - 60 atm of internal pressure. Phages and viruses have evolved diverse strategies to strengthen their capsids, such as non-covalent binding of auxiliary “decoration” proteins. The P22-like phages are paradigms for understanding the biophysics of capsid assembly and maturation. For example, phage L, Dec protein that has a highly unusual binding strategy where precisely distinguishes between nearly identical regions of the capsid. We combine cryo-electron microscopy and three-dimensional image reconstruction at near atomic resolution, with molecular dynamics techniques to discern the structure of native phage L particles. We used NMR to determine the structure/dynamics of Dec in solution. Key regions of coat and Dec that modulate the selectivity of Dec binding are elucidated.

Introduction

Viral icosahedral capsids are formed from multiple copies of a single or a few types of coat proteins that encapsidate the genome. Because of the symmetry of capsids that have more than 60 coat subunits, genetically identical proteins must assemble into capsid sites with different quasi-equivalent conformations, such that some coat proteins are in hexameric conformations and some are in pentameric conformations [1]. The resulting capsid shells often have additional decoration proteins bound to their exteriors that stabilize the virion against environmental insults. How decoration proteins bind to specific sites on quasi-equivalent capsids is poorly understood.

At least 10^{31} viruses are found in the biosphere [2], with double stranded DNA (dsDNA) bacteriophages being the most abundant. The majority of dsDNA containing phage virions have genomes enclosed in a pseudo-icosahedral capsid in which a tail that specifies host binding breaks the icosahedal symmetry. Members of the short-tailed phages (family *Podoviridae)* in the P22-like phage group, are a particularly well-studied model for understanding the biophysical mechanisms of capsid assembly [3] and capsid protein structures at near-atomic level detail [4,5]. The coat proteins of the P22-like phages, like all currently known tailed phages and herpesviruses, share a canonical HK97-like coat protein fold, one of the most ubiquitous protein folds in nature [6,7].

Tight packing of the dsDNA genome into the virion creates enormous internal pressure within the capsid, results in a high-energy state that primes the particles for infection, and facilitates delivery of the majority of the viral genome into the host. Phages have evolved diverse strategies to strengthen their capsids against internal pressures resulting from packaging of their genomes. A well-studied example is the phage HK97, where the coat protein forms covalent crosslinks with neighboring subunits, thereby creating a unique “chainmail” lattice [8]. In some other phages, a separately expressed auxilliary “decoration” protein (sometimes called “cementing” protein) functions as a molecular staple to stabilize mature capsids. The essential phage λ decoration protein gpD stabilizes its capsid by binding at all three-fold symmetry axes [9,10]. Conversely, many related phages do not utilize covalent crosslinks for stability, or auxillary decoration proteins. Instead, these capsids rely entirely on stabilizing interactions between protein subunits. For example, some coat protein P-loops create stabilizing interactions with neighboring capsid subunits around three-fold symmetry axes in the absense of auxiliary proteins [11-15]. The reasons why some phages require stabilization mechanisms such as auxiliary proteins, and others do not, despite using highly similar functional capsid building blocks remain poorly understood.

84 The coat proteins of phage L and phage P22 share 99.6% identity, but only phage L
85 encodes the small auxillary decoration protein, Dec [16]. Phage L and P22 encapsidate
86 similar length genomes and have similar capsid diameters. Therefore, the internal pressures
87 within both capsids are likey to be similar. Dec binds to P22 capsids *in vitro* with nanomolar
88 affinity at the same sites as on phage L virions, and increases the stability of P22 capsids at
89 elevated temperatures when treated with a Mg^{++} chelator *in vitro* [16,17]. Given this, the
90 role(s) of Dec in the life cycle of phage L compared to P22 is not immediately obvious, and,
91 unlike gpD in phage λ, Dec is not essential to withstand genomic packaging forces in phage
92 L virions (E. Gilcrease and S. Casjens, unpublished).
93 Dec binds only to mature particles, and not precursor procapsids [16] indicating that
94 it recognizes the specific surface topology of mature capsids. P22 and phage L capsids are
95 organized with a T=7 capsid geometry and have 11 vertices formed by coat protein pentons
96 and an additional 60 hexons to create the capsid. The twelfth penton vertex is occupied by
97 the portal channel that connects the phage virion to the tail apparatus. A T=7 organization
98 results in different protein landscapes between neighboring capsomers (Figure 1A). For
99 example, at the center of each of the 20 capsid facets there is a highly symmetric trimeric
100 interaction formed by the three surrounding hexons (called the "true three-fold" axis; black
101 traingle in Figure 1A). Between other hexons, there are "quasi-three-fold" symmetry axes,
102 which have a sublty different arrangement than the true fold symmetry axes (magenta circle
103 in Figure 1A). This quasi-three-fold site is less symmetric, and has bent contacts between
104 capsomers when compared with the true-three-fold symmetry site. Lastly, there is a second
105 type of quasi-three-fold symmetry site that occurs between hexons and the pentons (green
106 traingle in Figure 1A). The tight binding (~nM affinity) of Dec occurs at only quasi-three-fold
107 axes between hexons. Binding to the 20 true three-fold symmetry axes only occurs weakly,
108 with at least an order of magnitude lower affinity [18]. The latter is sufficiently low that these
109 sites are very sparsely occupied by Dec in the native phage L particles. No binding has

been detected at the quasi-three-fold sites surrounding the pentons [17,18]. Dec's ability to bind discriminately is in sharp contrast with the decoration proteins of other phages that fully saturate all symmetry-related sites in mature virions. Understanding the different mechanisms by which decoration proteins, such as gpD and Dec, can bind to surfaces of viral particles is not only important for understanding the principles of the underlying biology, but is also critical for structure-guided design of virus-inspired nanomaterials [18-23]. Here we investigate how Dec is able to distinguish these subtly different binding sites with high specificity.

We report the capsid structure of the phage L virion, and elucidate the mechanism of the selective binding by Dec. We use a combination of structural approaches including: 1) near atomic resolution cryo-electron microscopy (cryo-EM) and three-dimensional image reconstructions (3DR) of native phage L particles, 2) computational modeling of the Dec trimer when bound to the capsid refined using fully atomistic molecular dynamics (MD) simulations, and 3) nuclear magnetic resonance (NMR) structure and dynamics of Dec in solution. Dec displays significant asymmetry and flexibility when bound to capsids. The N-terminal globular domain of the protein that is in contact with the capsid has an Oligonucleotide/oligosaccharide-Binding (OB-fold; [24]) structure, and the C-terminal portion of Dec is comprised of a putative three-stranded β-helix domain. Several key residues within both the phage L coat protein lattice and the Dec trimer are predicted to modulate the selectivity of Dec binding. The contributions of these residues towards Dec binding were probed by site-directed mutagenesis. Our findings reveal that Dec has a novel protein fold for decoration proteins, and a binding mechanism that is not shared by other known phages and viruses.

Results

Cryo-EM structure of phage L at near-atomic resolution:

136 As a first step towards understanding the mechanism by which Dec binds to phage L,
137 we determined a near-atomic level resolution structure of native phage L capsids using cryo-
138 EM (Figure 1A). The resolution of the entire density map was determined to be 4.2 Å (see
139 Supplementary Materials, Figure S1). Both the overall protein structure, as well as the
140 specific contact points for attachment of Dec trimers to the coat protein subunits are clearly
141 discernable near quasi-three-fold symmetry axes between hexons. As anticipated from
142 previous studies [17,18], Dec very sparsely occupied true three-fold symmetry sites in phage
143 L virions, as there was only a hint of very weak density observed at these positions, and no
144 Dec occupancy was observed at quasi-three-fold sites between hexons and pentons.
145 Segmentation of the Dec density from the virion density map for subsequent analysis was
146 performed using UCSF Chimera's Segger [25] (Figure 1B, C). The native phage L capsid
147 map has been deposited in the EMDB database (accession number EMD-7787) along with
148 the capsid protein asymmetric unit (PDB ID 6D2F) and the Dec model (trimer from molecular
149 dynamic (MD)-based refinement against the cryo-EM map = PDB ID 6D2D).
150

151 **Structures of the phage L coat lattice and capsid-bound Dec trimers:**

152 As an initial guide for accurately fitting the phage L coat protein into the cryo-EM
153 density, we used the most recently deposited structure of a P22 coat protein asymmetric
154 unit (PDB ID: 5UU5; [26]), since phage L and phage P22 coat proteins are nearly identical,
155 with only four amino acid differences [17]. Upon initial docking, we found deviations between
156 the phage L capsid density and the P22 coat protein asymmetric unit. Therefore, to optimally
157 fit the cryo-EM density we built a model of the phage L coat protein lattice where each
158 capsid protein was allowed to move independently in the cryo-EM density envelope during
159 MD-based refinement instead of assuming perfect icosahedral symmetry (Figure S2 panels
160 A-C). The phage L capsid protein domains are named as defined in [26,27] for P22 coat
161 protein. The amino acid sequence differences between phage L and P22 coat proteins were

162 accounted for during modeling; the R101H side chain is located in the spine helix pointing
163 towards the capsid interior, I154L is located in the A-domain towards the hexamer center,
164 M267L is in the I-domain, adjacent to but not interacting with Dec, and A276T in also located
165 in the I-domain but on the distal end pointing towards center of the hexamer (Figure S2D).
166 Overall, there were minor differences between the optimally fit P22 and phage L capsid
167 lattices. The phage L coat protein chains deviate from those in the P22 structure (PDB
168 5UU5) by about 1 Å for the hexamer and 1.5 Å for the penton unit, which is in the range of
169 what may be expected for structures of homologous proteins [28] (see Supplementary
170 Materials, Table S1, for the complete measurements).

171 At lower resolution, the capsid-bound Dec trimer was previously found to have a
172 tripod shape with three N-terminal legs interacting with the capsid surface and a protuding
173 central C-terminal head or stalk [17,18]. Our results agree with the previously published
174 structure, but the higher resolution map attained in this work allowed us to accurately model
175 the majority of the Dec protein and to identify the specific amino acids in both Dec and coat
176 protein that create the binding interface. The electron densities within the entire virion map
177 were assessed by local resolution analysis [29] (Figure S3). The segmented trimeric Dec
178 densities are asymmetric but well defined at the quasi-three-fold symmetry axes between
179 hexons [18,20] (Figure 1A). The resolution within the Dec density is on average lower than
180 the capsid, likely due to protein flexibility, especially in the C-terminal stalk region (Figure
181 S3).

182 The Dec protein fold was determined by first using homology modeling (see
183 Materials and Methods for details) followed by a fully atomistic refinement fit to the
184 segmented cryo-EM density using MD-based fitting (Figures 1C, and S4). In brief, the N-
185 terminal domain was modeled using an OB fold (described in more detail below) and the C-
186 terminal domain with a three-stranded β-helix domain. The presence of an OB fold was
187 identified by homology and a template-based model was initially docked into the cryo-EM

188 density envelope. Studies using NMR also revealed an OB fold from Dec monomers, not
189 bound to the capsid (see NMR section below). The final trimeric Dec structure was refined
190 using MD-based flexible fitting within the cryo-EM density envelope, using the NMR
191 constraints to generate the final Dec structure.

192 The N-terminal domain of Dec (residues 10-88) was well defined by the cryo-EM
193 density, but residues 89-134 were predicted with a lower confidence owing to the flexibility
194 and lower resolution within that portion of the structure (Figures S3, S4). As we previously
195 observed [18], the N-terminal domain forms the legs of the Dec "tripod" that are bound to the
196 capsid, and the C-terminal region forms its protruding central stalk. As discussed in more
197 detail below, the C-terminal domain appears to be involved in trimerization, while the N-
198 terminal domains have little or no inter-subunit contacts within the trimer.

199

200 **NMR structure of the Dec monomer has an OB-fold domain and an unfolded C-**
201 **terminus:**

202 To further investigate the properties of Dec, we characterized the unassembled
203 protein in the absence of capsids by solution NMR. Initial NMR spectra of Dec at neutral pH
204 gave extremely broad lines, with poorer signals than expected for a 43 kDa trimer, which
205 was likely due to aggregation. We were able to achieve reproducibly good samples that
206 gave NMR spectra with sharper lines using a protocol [30] in which Dec is acid-unfolded by
207 lowering the pH to 2, followed by a refolding step induced by adjusting the pH to 4.
208 Subsequent characterization of the protein using size exclusion chromatography, native-gel
209 electrophoresis, and ^{15}N NMR relaxation measurements (Figure S5A) showed that the
210 unfolding/refolding protocol converts purified Dec from a trimer to partially folded monomers
211 [30]. The refolded Dec monomers were stable for about a week after refolding but exhibited
212 NMR line broadening, indicative of slow folding/oligomerization and aggregation after longer
213 times at pH 4 or higher.

The good quality of the NMR data obtained following the acid-unfolding/refolding protocol, enabled us to obtain nearly complete (98%) NMR assignments for the monomeric Dec protein [30]. The NMR structure was determined using the program ARIA 2.3 [31], based on the experimental NMR constraints summarized in Table 1. The coordinates of the Dec monomer NMR structure ensemble have been deposited to the PDB under accession number 6E3C.

The N-terminal domain of the Dec monomer has an OB-fold motif (Figure 2). The NMR structure thus determined is close to an initial NMR model calculated with the program CS-ROSETTA [32], based on the assigned NMR chemical shifts in combination with template-based modeling (Figure S5). The backbone (Cα, C', N, O) RMSD is 2.3 Å over the folded parts of the structure (residues 12-89) between the NMR structure and the CS-Rosetta model. Submission of the NMR Dec monomer structure to the DALI server [33] identified about 80 matches to proteins that contain similar OB-fold domain structures. The strongest of these is a portion (residues 117-174) of chain E of the 40S ribosomal protein SA (PDB code 4KZX-E). This superposed on the Dec NMR structure with an Cα RMSD of 3.5 Å over 61 residues, supporting our interpretation that the structure of the Dec N-terminus is in the OB-fold family.

The canonical OB-fold motif [24] is a five-stranded Greek Key β-barrel, comprised of a β1-β3 meander and a β4-β5 hairpin, with an α-helix 'αOB' intervening between strands β3 and β4 (Figure 2A). The five-stranded OB-fold β-barrel is closed by an antiparallel pairing between strand β1 and β4, and a short parallel pairing between stands β3 and β5 [24]. In the Dec structure the anti-parallel pairing of stands β1 and β4 is conserved, but strands β3 and β5 are too distant (~ 13 Å) for any H-bond contacts. Thus, the Dec β-sheet is distorted to a more open structure compared with the classical five-stranded OB-fold β-barrel (Figure 2B). In general, the cores of OB-fold β-barrels are consolidated by three layers of hydrophobic

239 residues [24,34]. This arrangement is also present in the Dec structure (not shown). The
240 canonical role of the helix αOB is to provide a 'hydrophobic plug' for the bottom hydrophobic
241 layer of the β-barrel [24,34]. Residue V55 appears to serve this role in Dec. In OB-fold
242 proteins the orientation of the helix αOB is more variable than that of the β-barrel [35,36],
243 and in Dec, the αOB helix extends almost directly between strand β3 and β5, with the helix
244 axis in the plane of the β1-β3 meander, rather than below this structure (Figure 3B).

245 As with many OB-fold proteins [36], Dec has additional non-conserved elements of
246 secondary structure at the periphery of the conserved motif. The short strand β0 forms an
247 anti-parallel pair with the N-terminus of the OB-fold strand β1, and the helix αC extends
248 away from the last OB-fold strand β5 (Figure 2C). Outside of the folded globular part of the
249 Dec monomer structure, residues 1-11 and 90-134 are disordered (Figure 2B). Although
250 these segments were included in the NMR structure calculations, they have no defined
251 structure in the Dec monomers (Figure 2B). The NMR structure agrees well with the model
252 of trimeric Dec derived from MD-based flexible fitting within the cryo-EM density, with a
253 range of RMSDs of 2.0-2.6 Å for the folded parts of the protein (residues 12-86), and 1.4-1.7
254 Å for the OB-fold portion of the structure (residues 20-77) (Figure 3, movie S1).

255 To further characterize the dynamics of Dec, we collected NMR ^{15}N-relaxation data
256 (Figure S5) and analyzed the dynamics of the monomeric protein in terms of the "Model-
257 Free" formalism. The local backbone mobility of the Dec monomers is summarized in Figure
258 4. The N-terminus from residues 1-11 and the C-terminus from residues 90-134 have small
259 S^2 order parameters characteristic of unfolded protein segments (Figure 4A). The random
260 coil chemical shifts of these regions [30] and the lack of long-range NOEs, are also
261 consistent with these regions being unstructured in the Dec monomers. Small and
262 intermediate S^2 values indicative of increased flexibility on the ps-ns timescales are also
263 seen at sites within the folded globular portion of Dec (Figure 4A). Information on motions

264 within slower μs-ms timescales can be garnered from exchange contributions to R2
265 transverse relaxtion ($R2_{EX}$ parameters). The sites with the largest $R2_{EX}$ contributions are
266 similar to those with low S2 order parameters, in particular L2-3, L4-5, and the region
267 surrounding the loop L3-α (purple and red in Figure 4B). The sites within the folded portion
268 of the Dec monomers that have the largest flexibility based on the S^2 and $R2_{EX}$ are shown in
269 Figure 4 C,D, respectively.
270

271 **Mutagenesis of P22 coat protein and Dec reveals key residues that modulate binding:**

272 The cryo-EM map of the native phage L virion allowed us to fit models of both Dec
273 and coat protein to visualize the binding interface. The resolution of the map in this region
274 was sufficient to fit some bulky side chains to the coat and Dec proteins. Analysis of the
275 binding interface revealed several residues in close contact between the phage L coat
276 protein and the Dec trimer that appear to be important for binding. Previous work suggested
277 that Dec binding to P22 capsids is driven primarily through electrostatic interactions [20],
278 and our data suggests a highly charged binding interface (Figure 5).

279 To assess the role that specific coat protein surface residues play in modulating Dec
280 binding, the following five coat protein residues in potential close contact with Dec were
281 chosen for single amino acid substitution by site directed mutagenesis: E81R, P82S, R299E,
282 P322S, and E323R (Figure 5; Supplementary Materials, movie S3). Site directed
283 mutagenesis was performed on a plasmid that expresses P22 coat protein (see Materials
284 and Methods) as described previously [37-39]. Cells carrying the plasmid were infected with
285 P22 phages having an *amber* mutation in gene *5* (encodes coat protein), so that any phages
286 produced are the result of complementation from the coat gene expressed from the plasmid.
287 None of the amino acid substitutions affected virion production; phages assembled with
288 each coat protein variant were grown to high titer and and were phenotypically
289 indistinguishable from the parental phage.

290 We noted that coat proteins occupying different local conformations (as a result of
291 the quasi-equivalent capsid lattice) contribute different residues to the binding interface
292 (Figure 5A, Movie S3). For example, residues E81, P82, and R299 from the coat protein
293 subunits that form the quasi-three-fold symmetry axes (grey subunits in Figure 5) contact
294 Dec, whereas residues P322 and E323 contact Dec from adjacent and overlapping coat
295 protein subunits (black subunits in Figure 5). While their closeness to Dec clearly indicates
296 that it interacts near these coat residues, there are no obvious salt bridges between the coat
297 protein and Dec molecules based on the MD experiments. To assess the role that specific
298 Dec residues play in capsid binding, we also made five single amino acid substitutions in
299 recombinant phage L Dec protein: K30D, Y31A, Y49E, Y71A, and E73R (see Materials and
300 Methods). Modified Dec proteins were added to WT P22 mature phage particles, complexes
301 were purified using CsCl gradients, and relative amounts of Dec protein bound to virions
302 were quantitated. The global secondary structure of all Dec variants was indistinguishable
303 from the WT protein by circular dichroism. Furthermore, native gel experiments performed
304 as described previously [30] show that all Dec variants assemble as trimmers in solution.
305 Therefore any changes in Dec occupancy in the variants are likely due to a disruption of the
306 binding interface, rather than protein folding aritfacts.

307 Among the five coat protein changes, coat amino acid substituions E81R and E323R
308 attenuated but did not completely abolish Dec binding ability (Figure 5 B,C). Therefore, we
309 created a variant containing both amino acid substitutions, E81R:E323R. This coat protein
310 variant displayed less Dec binding than each of the individual substitutions; however,
311 residual Dec binding was still detected. Our data suggest that since the capsid quasi-three-
312 fold binding sites for Dec are formed by coat proteins in two distinct quasi-equivalent
313 conformations, weaker Dec binding (<20%) can still occur when this interface is disrupted,
314 even by two amino acid substitutions. In addition, amino acid subtitutions in Dec K30D and

315 Y49E displayed lower binding than the WT protein, consistent with the prediction of an
316 electrostatic binding interface (Figure 5D, Movie S3).

317 The close contact region between Dec and coat can be thought of as including two
318 binding sites. One includes coat residues E81 and P82 along with their closest interacting
319 Dec residues K30, Y31 and Y49 (Figure 5D, “site 1”). For example, Dec residue Y49 is
320 pointed directly towards the side chain of coat residue E81. The other patch includes Dec
321 residues Y71 and E73 and coat residues P322, E323 and R299 (Figure 5D, “site 2”). Overall,
322 variations in site 1 had the largest effect on binding. In Dec, site 1 residues K30 and Y49
323 had the largest effect on binding saturation, and in coat protein site 1 residue E81R had the
324 largest effect relative to the other substitutions. Although site 1 clearly plays a strong role in
325 modulating Dec binding, coat residue E323R which resides in site 2 had a reproducible,
326 albeit modest effect. We conclude that the first site plays a substantially larger role in
327 mediating Dec binding to coat protein, and is largely due to electrostatic interactions, when
328 compared with the second site.

329 Not all of the variations tested in coat protein reduced binding, namely P82S, R299E
330 and P322S (we intentionally made conservative proline substitutions as coat protein is
331 highly aggregation prone [4]). Additionally, not all of the variations tested in Dec reduced
332 binding, including Y31A, Y71A, and E73R. These observations are consistent in light of the
333 3D capsid structure. Coat protein residue P82 is at a lower virion radius than E81 and likely
334 too far from the Dec residue Y49 to affect binding when it is altered. Coat protein change
335 R299E did not alter binding, and this is consistent with the fact that when the closest
336 adjacent Dec residue Y31 is changed to an alanine there was also no effect on binding.
337 Lastly, coat residue P322 forms an interface with two Dec residues, Y71 and E73, and
338 single subsitutions at any of these positions have no effect on binding. Even though the
339 cryo-EM density is strong in this region indicating protein:protein contact, electrostatic
340 interactions may not be the driving force at site 2, but instead weaker interactions such as

341 van der Waals could contribute to binding. Further experiments will be required to fully
342 characterize any subtle changes in binding affinity of the variants that did not obviously
343 decrease binding saturation here.

344 Given that the binding interface is comprised of coat protein subunits in two distinct
345 quasi-equivalent conformations, other weak protein-protein interactions may help promote
346 binding at site 2, which was not dramatically affected by our mutagenesis. Consistent with
347 this result, mutational analysis of the gpD decoration protein in phage λ shows that
348 "numerous and redundant non-covalent binding interactions" are important for the binding
349 and capsid stabilization mechanism, and that changes in binding are not solely based on
350 single, critical residues [40]. Though gpD and Dec have different folds (see Discussion),
351 perhaps multiple, redundant binding interactions are a common theme among capsid
352 decoration proteins.

353

354 **A structural basis for the discminatory binding of Dec to capsids**

355 We compared the observed interaction of Dec trimers with the capsid at the quasi-
356 three-fold and one computationally placed at the point of very weak Dec density at the true
357 three-fold symmetry axis using MD-based simulations (Figure 6). Overall, the interactions
358 with Dec at the different capsid sites are very similar, but Dec modeled at the true three-fold
359 axis is tilted further away relative to the capsid. Moreover, the potential MD-modeled
360 contacts between Dec and coat protein at the true three-fold axis are not as close as the
361 observed contacts at the true three-fold axes (see close-ups in Figure 6C and 6D). This is
362 consistent with the reduced binding affinity of Dec at true three-fold axes and the only very
363 weak density observed in our cryo-EM reconstructions at that site.

364

365

366 **Discussion**

367

368 **Decoration proteins employ a variety of binding schemes to adhere to phage capsids:**

369 For dsDNA tailed phages and related viruses, decoration proteins can occupy the
370 capsid lattice in several different positions. Some bind capsids at the center of hexamers
371 including decoration proteins in phages T4, T5, RB49, and Sf13 through Sf19, [41-44].
372 Alternatively, some decoration proteins bind the edges of hexamers as exemplified by gp17
373 in phage N4 [45]. Others, bind the capsid in areas between capsomers such as gpD in λ,
374 gp56 in phage TW1, Soc in phage T4, gp87 in phage P74-26, and Dec in phage L [9,17,46-
375 48]. In all of the aforementioned cases, the decoration proteins are added after capsid
376 assembly. Conversely, the herpesvirus heterotrimeric triplex protein decorates the outside of
377 the capsid and is also essential during capsid assembly. For the majority of these examples,
378 all possible quasi-equivlent binding sites on the lattice are occupied by the decoration
379 proteins. By contrast, in phage L, Dec only binds at one type of symmetry axis with high
380 affinity: the quasi-three-fold sites between hexamers (Figure 1A).

381 To function in a stabilizing capacity, decoration proteins must bind capsids with high
382 enough affinity to remain associated even under harsh environmental conditions.
383 Interestingly, the requirement for binding affinity must be balanced with binding specificity to
384 allow discrimination between binding sites. Indeed there is a wide range of reported K_Ds for
385 various decoration proteins. Phage L's Dec and T4's Hoc bind their respective capsids with
386 nM affinity, whereas pb10 binds phage T5 with pM affinity [18,41,49]. Taken together,
387 variations in binding affinities and saturating versus discriminating binding behavior
388 suggests that decoration proteins are capable of recognizing subtle differences in capsid
389 lattices. The reason some decoration proteins descriminate between similar quasi-
390 equivalent sites is unknown, but some positions on the capsid lattice may be more
391 vulnerable to environmental assaults than others, therefore some positions may not require
392 stabilization from a decoration protein.

393

394 **Dec has a novel architecture:**

395 In dsDNA tailed phages, previously studied decoration proteins for which atomic-
396 resolution structures are known have two basic types of protein folds. For decoration
397 proteins such as phage T5's pb10 and T4's hoc, the overall fold is that of an Ig domain
398 [41,44]. A second, more common type of decoration protein, exemplified by phage lambda's
399 gpD, P74-26's gp87, phage 21's SHP, and TW1 gp56, binds capsids at all local three-fold
400 axes between capsomers. These proteins have similar polypeptide folds and form a
401 symmetric trimer with an N-terminal β-tulip domain and an α/β subdomain that binds and
402 stabilizes capsids through hydrophobic interfaces [40,48]. Our work shows that Dec
403 represents a third type of decoration protein fold (Figure 7), the OB-fold, as well as a
404 different capsid-binding mechanism that discriminates quasi three-fold capsid binding sites
405 in favor of true three-fold sites. To our knowledge, Dec represents the first occurence of an
406 OB-fold structure in a virus decoration/cementing protein.

407 Crystal structures for gpD [50], gp87 [48], and SHP [51] lack resolution for several N-
408 terminal residues, indicating that these regions are flexible when these decoration proteins
409 are not associated with capsids. Cryo-EM maps of gpD in native phage λ show that the N-
410 terminus becomes highly ordered when gpD is in a bound conformation, and that the N-
411 terminus is the major part of the capsid binding mechanism as the N-terminus forms a
412 stabilizing β-sheet with strands supplied from the capsid protein [9]. Like gpD, the N-
413 terminus of the Dec monomer is disordered in solution as shown here by NMR. However,
414 unlike gpD, our data indicates that the Dec N-terminus remains rather flexible in the capsid-
415 bound form since there is (1) no cryo-EM density that is attributable to the first 10 residues,
416 (2) our previous cryo-EM data show the N-terminus of Dec can be labeled with large cargo
417 such as nanogold beads that are rather flexibly bound to the capsid [18], and (3) deletion of

418 the first 11 residues of Dec does not affect capsid binding afiinity [20]. When we compare
419 the phage L Dec binding motif to the capsid stabilization mechanism in HK97, we see that
420 the residues that control Dec binding occupy similar spatial positions as the HK97 catalytic
421 residues that crosslink to form the lattice "chainmail". Furthermore, comparison of Dec to the
422 β-tulip family decoration proteins highlights some interesting implications about binding
423 affinitiy and selectivity of binding locations in terms of symmetry of the auxiliary proteins
424 involved. Perfect trimeric symmetry seems to allow for a broader binding specificity. For
425 example, highly symmetric trimers in gpD and gp87 allow these decoration proteins to
426 occupy all quasi-equivalent binding sites including true three fold symmetry axes and also
427 both types of quasi-three-fold sutes. By contrast, the inherent asymmetry in the Dec trimer is
428 an unusual property among decoration proteins and seems to modulate Dec binding
429 selectivity to only one type of symmetry axis. Dec appears to represent a new evolutionary
430 lineage of decoration proteins that is distinctly different than those in the β-tulip family and
431 whose capsid binding is similarly driven mainly by electrostatics in site 1, with some van der
432 Waals interactions contributing to binding in site 2.
433
434 **Summary**
435 Phage L Dec protein has an N-terminal OB domain, and a C-terminal β-helix domain.
436 Capsid stabilization occurs through electrostatic interactions between Dec and coat protein
437 subunits. Discriminiatory binding occurs at the quasi-three-fold symmetry axes between
438 hexons and not the true-three symmetry sites largely due to surface area of contact with the
439 capsid protein. Dec has a novel fold and capsid stabilization mechanism compared to other
440 known decoration proteins.
441
442 **Materials and Methods**

443

444 **Strains and media:** Phage L, its bacterial host, and purification procedures to produce high-
445 titer stocks were previously described [16,17]. Stocks were stored in a 10 mM Tris (pH 7.6)
446 and 10 mM $MgCl_2$ buffer. LB Miller broth and LB agar (Invitrogen) were used for all
447 experiments.

448

449 **Purification of P22 phage with various coat proteins:** *Salmonella enterica* serovar
450 Typhimurium strain DB7136 (leuA414am, hisC525am, su^0), expressing P22 coat protein
451 from mutant pMS11 plasmids, were infected with P22 phage carrying amber mutations in
452 gene *5* to stop production of phage-encoded coat protein as described previously [39]. This
453 P22 strain also carried the c1-7 allele to prevent lysogeny. The resulting phages containing
454 amino acid substitutions in coat protein, were purified using standard protocols [16,18].

455

456 **Site-directed mutagenesis of P22 coat protein and phage L Dec protein:** The plasmid
457 pMS11 was mutated using Quikchange protocols as described previously [52] to generate
458 plasmids that express coat protein containing the following substitutions: E81R, P82S,
459 R299E, P322S, E323R, E81R:E323R. All plasmids were Amp^R (100 μg/mL) and IPTG
460 inducible (1 mM). Sequences were confirmed at the RSTF Genomics Core at Michigan
461 State University. Plasmid pDec was mutated using Quikchange protocols, and was used to
462 express wild type and variant Dec, each with a C-terminal histidine tag. Phage P22
463 purification [16,18] and binding assays were performed as described [17,18]. To measure
464 binding, purified Dec was added to P22 phages made with WT or variant coat proteins. Free
465 Dec was separated from Dec bound to P22 particles by cesium chloride density gradient
466 sedimentation as previously described [16,17]. Bands containing P22 were TCA-precipitated,
467 and analyzed by SDS-PAGE. Coomassie-stained gel bands corresponding to P22 coat
468 protein and Dec were quantitated and normalized to the ratio found in native P22 particles

469 when bound with Dec. All binding experiments were repeated two to four times.
470 Representative data are shown.
471

472 **Cryo-EM:** Aliquots (~5 μL) of phage L virions were vitrified and examined using published
473 procedures [53]. Briefly, this involved applying samples to Quantifoil R2/2 holey grids that
474 had been plasma cleaned for ~20 sec in a Fischione model 1020 plasma cleaner. Grids
475 were then blotted with Whatman filter paper for ~5 sec, and plunged into liquid ethane.
476 Samples were pre-screened for concentraton and purification quality in a JEOL JEM-
477 2200FS TEM using a Gatan 914 specimen holder, using standard low-dose conditions as
478 controlled by SerialEM [54]. High-resoluiton imaging on an FEI Titan Krios was performed at
479 Florida State University. Micrographs were recorded on a Direct Electron DE-20 camera wth
480 a capture rate of 25 frames per second using a total of 53 frames, and a final dose of ~27
481 e/Å^2 at a final pixel size of 1.26 Å. Movie correction was performed using the Direct Electron
482 software package, v2.7.1 [55] on entire frames.

483 **3D image reconstructions of icosahedral particles:** Micrographs exhibiting minimal
484 astigmatism were selected for further processing. The objective lens defocus settings used
485 to record each data set ranged 0.35 to 2.49 μm. In total, the final reconstruction used 7,879
486 of the best particles from 494 images. The program RobEM
487 (http://cryoEM.ucsd.edu/programs.shtm) was used to estimate micrograph defocus and
488 astigmatism, extract individual phage L particles, and to preprocess the images. 150 particle
489 images were used as input to the random-model computation procedure to generate an
490 initial 3D density map at ~25 Å resolution [56]. Each map was then used to initiate
491 determination and refinement of particle orientations and origins for the complete set of
492 images using the current version of AUTO3DEM (v4.01.07) [57]. Phases of the particle
493 structure factor data were corrected to compensate for the effects caused by the microscope

494 contrast-transfer function, as described [58]. The Fourier Shell Correlation ($FSC_{0.5}$) "gold
495 standard" criterion was used to estimate the resolution of the final 3D reconstructions [59].
496 Graphical representations were generated using the UCSF Chimera visualization software
497 package [60]. Local resolution was estimated as previously described [29]. Map
498 segmentation was performed using the Segger tool in Chimera [60].
499
500 **Molecular dynamics-based flexible fitting of capsid-bound Dec:** Initial structures of the
501 capsid proteins except Dec were built via homology modeling based on the available
502 structure for P22 (PDB ID 5UU5 [26]). Using the symmetry operations in the PDB structure,
503 1/8th of the capsid was constructed to cover the entire cryo-EM density map for phage L.
504 Even if only part of a capsid protein copy was needed to cover the map, the entire protein
505 was retained so that some capsid proteins extended beyond the volume covered by the
506 density map. To obtain an initial structure, the entire capsid complex was fitted via rigid-body
507 docking to the density map using UCSF Chimera [60].
508 The initial model for Dec was assembled in multiple stages. Secondary structure
509 prediction for the Dec sequence suggests a predominantly β-sheet structure with some α-
510 helical content. A search with PSI-BLAST [61] for known structural homologs of the Dec
511 sequence did not result in any hits with sufficiently reliable E-values (<0.1). NMR chemical
512 shift data for Dec also indicate a fold consisting mostly of β-sheets and two α-helices in the
513 N-terminal part of Dec [30]. Based on the NMR chemical shifts, eleven initial models were
514 built via CS-ROSETTA [32]. All of the resulting models feature an OB-fold, consistent with
515 the predicted secondary structure and resulted in three-dimensional structures that fit
516 approximately into the cryo-EM densities for Dec with good matches to the helical and
517 strand regions that are clearly identifiable in the EM density map. The CS-ROSETTA [32]
518 model that initially fit the EM density best was selected for further modeling. Initial trimer

519 models guided by the EM densities were constructed covering residues 11 to 88 and
520 subsequently fit to the segmented EM density for Dec only via energy minimization (over
521 1,000 steps) and short molecular dynamics (2,000 steps at 100K, 5,000 steps at 200K, and
522 5,000K steps at 300K) followed by minimization again (1,000 steps) using the EMAP facility
523 [62] in CHARMM (version 42a2) [63]. A distance dependent dielectric was applied to
524 approximate an aqueous solvent environment. During the minimization, distinct structural
525 elements (28 - 62, 12 - 26 and 63 - 77, and 79 - 86) were restrained separately so that they
526 could move relative to each other in order to improve the fit to the EM density. All of the
527 restraints were applied just to Cα coordinates allowing the rest of the backbone and side
528 chains to move freely during the optimization.

529 After initial optimization of the N-terminal part of Dec, the N-terminus was extended
530 to residue 1 using an extended chain, a linker was added to cover residues 89-92, and a
531 homology model for the C-terminus based on a fragment from the bacteriophage T4
532 proximal long tail fibre protein gp34 (PDB ID: 4UXE [64]) was added. The EM density lacks
533 sufficient resolution for reliably modeling the C-terminal part of Dec in terms of side chain
534 orientations but indicates a barrel-shaped structure consistent with a β-helix seen in many
535 bacteriophage tail structures. The modeled β-helix is also consistent with the secondary
536 structure predicted for the C-terminus of Dec from its sequence [17,18,30]. The selection of
537 this structure as a template was based on the dimension of the β-helix that was narrower
538 than most β-helices found in other tail structures, and in better agreement with the EM
539 density. The complete model of the Dec trimer was then re-optimized against the EM density
540 with the same protocol as before, allowing the C-terminal part of the trimer to move
541 separately from the N-terminus to find the best fit to the EM density. We note, that while the
542 model for the N-terminal part of Dec is supported by NMR data and a good fit to the
543 relatively high resolution EM density, the model for the C-terminus is speculative due to a
544 lack of high-resolution experimental data.

545 The initial Dec model was combined with six capsid proteins at the quasi-three fold
546 symmetry axis, and re-optimized via energy minimization to improve the fit at the interface
547 between Dec and the capsid proteins. The optimized Dec model was further then combined
548 with a larger capsid complex covering 1/8th of the capsid. A copy of Dec was placed at each
549 quasi-three fold symmetry axis and an additional copy was placed at the true three-fold axis
550 as there was also faint EM density at the latter sites. The combined capsid-Dec complex
551 was finally subjected to extensive optimization against the EM density via molecular
552 dynamics based flexible fitting using NAMD (version 2.10b2) via the MDFF module [65].
553 NAMD was chosen at this stage for better parallel computing performance [66] since the
554 model of 1/8th of the capsid in full atomistic detail is quite large (>500,000 atoms). In the
555 refinement against the entire EM density, each capsid protein was restrained to its internal
556 conformation but allowed to move relative to other proteins. In addition, backbone torsions
557 and hydrogen bonds were restrained to maintain secondary structure elements. VMD [67]
558 was used to automatically setup the MDFF input. A simple constant dielectric environment
559 (ε=80) was used and after minimization over 1000 steps, molecular dynamics simulations
560 were carried out at 300K over 50,000 steps with a 1 fs integration time step. After a first
561 round of refinement, symmetry copies of Dec and the capsid proteins were averaged, and a
562 second round of refinement was carried out for the 1/8th capsid that started from the
563 averaged capsid and Dec units but allowing each unit to again move independently.
564
565 **NMR characterization of the structure and dynamics of monomeric Dec:** Samples of
566 recombinant Dec enriched in ^{15}N, ^{13}C and ^{2}H isotopes for NMR studies were expressed in *E.*
567 *coli* and purified as described [30]. To obtain samples suitable for NMR, 0.3 to 0.5 mM Dec
568 was unfolded to pH 2 for 20 min, followed by refolding to pH 4.0 in 20 mM sodium acetate
569 buffer containing 50 mM NaCl and 1 mM EDTA. The acid-unfolding/refolding procedure
570 converted Dec to a monomer as monitored by native gel electrophoresis and size exclusion

571 chromatography. All NMR data were collected for samples held at a temperature of 33 ^{o}C.
572 Virtually complete NMR assignments for monomeric Dec (> 98% of backbone resonances)
573 were obtained using a suite of 3D NMR experiments [30] and have been deposited in the
574 Biological Magnetic Resonance Bank (http://www.bmrb.wisc.edu/) with the accession
575 number 27435.

576 NMR structures for Dec were calculated with the program ARIA v. 2.3.1 [31] using
577 the experimental restraints summarized in Table 1. Backbone (ϕ,ψ) and sidechain (χ1)
578 torsion angles were calculated from assigned HN, N, Hα, Cα, Cβ, and CO NMR chemical
579 shifts using the program TALOS-N [32]. NOE-based distance restraints were obtained from
580 3D ^{15}N- and ^{13}C-NOESY experiments collected on ^{15}N/^{13}C-labeled Dec samples, with or
581 without 50% fractional deuteration. The NOESY experiments were collected on an 800 MHz
582 spectrometer equipped with a cryogenic probe, using a mixing time of 100 ms. Hydrogen
583 bond restraints were included based on H-bond donors and acceptors identified in a long-
584 range HNCO experiment [68] recorded on a ^{2}H,^{13}C,^{15}N triple-labeled Dec sample in TROSY
585 mode at 800 MHz, and H-bond donors inferred from amide proton protection in ^{1}H to ^{2}H
586 hydrogen exchange experiments. Water refinment in the program ARIA [31] was used as a
587 final optimization step for the NMR structures.

588 Backbone dynamics of Dec were characterized using ^{15}N NMR R1, R2, and ^{1}H-^{15}N
589 NOE relaxation data recorded at 800 MHz. R1 rates were obtained using interleaved
590 relaxation delays of 0.05, 0.13, 0.21, 0.49, 0.57, 0.71 and 0.99 s. R2 rates were determined
591 using interleaved relaxation delays of 0.01, 0.03, 0.05, 0.07, 0.09, 0.11, and 0.15 s. A 2 s
592 pre-acquisition delay was used for recovery to thermal equilibrium. ^{1}H-^{15}N NOE values were
593 determined from the ratio of crosspeak intensities in a spectrum for which the proton signals
594 were saturated for 2.5 s and a control spectrum in which the saturation period was replaced
595 by a pre-acquisition delay of equivalent length. The processing and analysis of relaxation
596 parameters was done according to published protocols [35]. Model-free analyses [69] of the

597 ^{15}N relaxation data were performed with the program Tensor2 [70], yielding an optimal global
598 isotropic rotational correlation time of 7.4 ns.
599
600 **Acknowledgements:** We thank Timothy S. Baker (University of California, San Diego),
601 Gabriel C. Lander and John E. Johnson (The Scripps Research Institute) for advice and
602 support during the preliminary phase of this project, Giovanni Cardone for support in the
603 local resolution analysis, Prof. Angela Gronenborn (U. Pittsburgh School of Medicine) for
604 useful discussion, and Anne R. Kaplan for help with NMR structure calculations of Dec. This
605 material is based upon work supported by the AAAS Marion Milligan Mason Award for
606 Women in the Chemical Sciences to KNP, by grants NIH GM084953 and GM126948 to MF,
607 NIH grant R01 GM076661 and a grant from the UConn Research Excellence Program to
608 CMT and ATA. High resolution cryo-electron microscopy data were collected at Florida State
609 University, and the FSU facility is supported by the following grants: S10 OD018142 and
610 S10 RR025080 under PI Ken Taylor.
611
612 **Competing Interests**
613 The authors have no competing interests to declare.
614
615 **References:**
616
617 1. Caspar DLD, Klug A (1962) Physical principles in the construction of regular viruses. Cold
618 Spring Harbor Symp Quant Biol 27: 1-24.
619 2. Bamford DH, Grimes JM, Stuart DI (2005) What does structure tell us about virus
620 evolution? Curr Opin Struct Biol 15: 655-663.
621 3. Parent KN, Zlotnick A, Teschke CM (2006) Quantitative analysis of multi-component
622 spherical virus assembly: Scaffolding protein contributes to the global stability of
623 phage P22 procapsids. J Mol Biol 359: 1097-1106.
624 4. Teschke CM, Parent KN (2010) 'Let the phage do the work': Using the phage P22 coat
625 protein structure as a framework to understand its folding and assembly mutants.
626 Virology 401: 119-130.

627 5. Parent KN, Schrad JR, Cingolani G (2018) Breaking Symmetry in Viral Icosahedral
628 Capsids as Seen through the Lenses of X-ray Crystallography and Cryo-Electron
629 Microscopy. Viruses 10.
630 6. Hendrix RW (2002) Bacteriophages: evolution of the majority. Theor Popul Biol 61: 471-
631 480.
632 7. Baker ML, Jiang W, Rixon FJ, Chiu W (2005) Common ancestry of herpesviruses and
633 tailed DNA bacteriophages. J Virol 79: 14967-14970.
634 8. Popa MP, McKelvey TA, Hempel J, Hendrix RW (1991) Bacteriophage HK97 structure:
635 wholesale covalent cross-linking between the major head shell subunits. J Virol 65:
636 3227-3237.
637 9. Lander GC, Evilevitch A, Jeemaeva M, Potter CS, Carragher B, Johnson, JE (2008)
638 Bacteriophage lambda stabilization by auxiliary protein gpD: timing location, and
639 mechanism of attachment determined by cryo-EM. Structure 16: 1399-1406.
640 10. Yang Q, Maluf NK, Catalano CE (2008) Packaging of a unit-length viral genome: the role
641 of nucleotides and the gpD decoration protein in stable nucleocapsid assembly in
642 bacteriophage lambda. J Mol Biol 383: 1037-1048.
643 11. Parent KN, Khayat R, Tu LH, Suhanovsky MM, Cortines JR, Teschke, CM, Johnson, JE
644 Baker TS. (2010) P22 coat protein structures reveal a novel mechanism for capsid
645 maturation: Stability without auxiliary proteins or chemical crosslinks. Structure 18:
646 390-410.
647 12. Chen DH, Baker ML, Hryc CF, DiMaio F, Jakana J, Wu W, Dougherty, M, Haase-
648 Pettingell, C, Schmid, MF, Jiang, W, Baker, D, King, JA, Chiu, W. (2011) Structural
649 basis for scaffolding-mediated assembly and maturation of a dsDNA virus. Proc Natl
650 Acad Sci U S A 108: 1355-1360.
651 13. Spilman MS, Dearborn AD, Chang JR, Damle PK, Christie GE, Dokland, T. (2011) A
652 conformational switch involved in maturation of *Staphylococcus aureus*
653 bacteriophage 80α capsids. Journal of Molecular Biology 405: 863-876.
654 14. Parent KN, Gilcrease EB, Casjens SR, Baker TS (2012) Structural evolution of the P22-
655 like phages: Comparison of Sf6 and P22 procapsid and virion architectures. Virology
656 427: 177-188.
657 15. Parent KN, Gilcrease EB, Casjens SR, Baker TS (2012) Structural evolution of the P22-
658 like phages: Comparison of Sf6 and P22 procapsid and virion architectures. Virology
659 427: 177-188.
660 16. Gilcrease EB, Winn-Stapley DA, Hewitt FC, Joss L, Casjens SR (2005) Nucleotide
661 sequence of the head assembly gene cluster of bacteriophage L and decoration
662 protein characterization. J Bacteriol 187: 2050-2057.
663 17. Tang L, Gilcrease EB, Casjens SR, Johnson JE (2006) Highly discriminatory binding of
664 capsid cementing protiens in bacteriophage L. Structure 14: 837-845.
665 18. Parent KN, Deedas CT, Egelman EH, Casjens SR, Baker TS, Teschke, CM. (2012)
666 Stepwise molecular display utilizing icosahedral and helical complexes of phage coat
667 and decoration proteins in the development of robust nanoscale display vehicles.
668 Biomaterials 33: 5628-5637.
669 19. Douglas T, Young M (2006) Viruses: making friends with old foes. Science 312: 873-875.
670 20. Schwarz B, Madden P, Avera J, Gordon B, Larson K, Miettinen, HM, Uchida, M,
671 LaFrance, B, Basu, G, Rynda-Apple, A, Douglas, T. (2015) Symmetry Controlled,
672 Genetic Presentation of Bioactive Proteins on the P22 Virus-like Particle Using an
673 External Decoration Protein. ACS Nano 9: 9134-9147.
674 21. McCoy K, Uchida M, Lee B, Douglas T (2018) Templated Assembly of a Functional
675 Ordered Protein Macromolecular Framework from P22 Virus-like Particles. ACS
676 Nano 12: 3541-3550.

677 22. Sharma J, Uchida M, Miettinen HM, Douglas T (2017) Modular interior loading and
678 exterior decoration of a virus-like particle. Nanoscale 9: 10420-10430.
679 23. Catalano CE (2018) Bacteriophage lambda: The path from biology to theranostic agent.
680 Wiley Interdiscip Rev Nanomed Nanobiotechnol.
681 24. Murzin AG (1993) OB(oligonucleotide/oligosaccharide binding)-fold: common structural
682 and functional solution for non-homologous sequences. EMBO J 12: 861-867.
683 25. Pintilie GD, Zhang J, Goddard TD, Chiu W, Gossard DC (2010) Quantitative analysis of
684 cryo-EM density map segmentation by watershed and scale-space filtering, and
685 fitting of structures by alignment to regions. Journal of structural biology 170: 427-
686 438.
687 26. Hryc CF, Chen DH, Afonine PV, Jakana J, Wang Z, Haase-Pettinggell, C, Jiang, W,
688 Adams, PD, King, JA, Schmid, MF, Chiu, W. (2017) Accurate model annotation of a
689 near-atomic resolution cryo-EM map. Proc Natl Acad Sci U S A 114: 3103-3108.
690 27. Rizzo AA, Suhanovsky MM, Baker ML, Fraser LC, Jones LM, Rempel, DL, Gross, ML,
691 Chiu, W, Alexandrescu, A, Teschke, CM. (2014) Multiple functional roles of the
692 accessory I-domain of bacteriophage P22 coat protein revealed by NMR structure
693 and CryoEM modeling. Structure 22: 830-841.
694 28. Eyrich VA, Marti-Renom MA, Przybylski D, Madhusudhan MS, Fiser A, Pazos, F,
695 Valencia, A, Sali, A, Rost, B. (2001) EVA: continuous automatic evaluation of protein
696 structure prediction servers. Bioinformatics 17: 1242-1243.
697 29. Cardone G, Heymann JB, Steven AC (2013) One number does not fit all: mapping local
698 variations in resolution in cryo-EM reconstructions. J Struct Biol 184: 226-236.
699 30. Newcomer RL, Belato HB, Teschke CM, Alexandrescu AT (2018) NMR assignments of
700 the phage-cementing protein Decorator. Biomol NMR Assign.
701 31. Bardiaux B, Malliavin T, Nilges M (2012) ARIA for solution and solid-state NMR.
702 Methods Mol Biol 831: 453-483.
703 32. Shen Y, Vernon R, Baker D, Bax A (2009) De novo protein structure generation from
704 incomplete chemical shift assignments. J Biomol NMR 43: 63-78.
705 33. Holm L, Rosenstrom P (2010) Dali server: conservation mapping in 3D. Nucleic Acids
706 Res 38: W545-549.
707 34. Alexandrescu AT, Gittis AG, Abeygunawardana C, Shortle D (1995) NMR structure of a
708 stable "OB-fold" sub-domain isolated from staphylococcal nuclease. J Mol Biol 250:
709 134-143.
710 35. Alexandrescu AT, Shortle D (1994) Backbone dynamics of a highly disordered 131
711 residue fragment of staphylococcal nuclease. J Mol Biol 242: 527-546.
712 36. Guardino KM, Sheftic SR, Slattery RE, Alexandrescu AT (2009) Relative stabilities of
713 conserved and non-conserved structures in the OB-fold superfamily. Int J Mol Sci 10:
714 2412-2430.
715 37. Parent KN, Suhanovsky MM, Teschke CM (2007) Phage P22 procapsids equilibrate with
716 free coat protein subunits. J Mol Biol 365: 513-522.
717 38. Suhanovsky MM, Parent KN, Dunn SE, Baker TS, Teschke CM (2010) Determinants of
718 bacteriophage P22 polyhead formation: the role of coat protein flexibilty in
719 conformational switching. Mol Micro 77: 1568-1582.
720 39. Suhanovsky MM, Teschke CM (2013) An intramolecular chaperone inserted in
721 bacteriophage P22 coat protein mediates its chaperonin-independent folding. J Biol
722 Chem 288: 33772-33783.
723 40. Lambert S, Yang Q, De Angeles R, Chang JR, Ortega M, Davis, C, Catalano, CE.
724 (2017) Molecular Dissection of the Forces Responsible for Viral Capsid Assembly
725 and Stabilization by Decoration Proteins. Biochemistry 56: 767-778.
726 41. Vernhes E, Renouard M, Gilquin B, Cuniasse P, Durand D, England, P, Hoos, S, Huet,
727 A, Conway, JF, Glukhov, A, Ksenzenko, V, Jacquet, E, Nhiri, N, Zinn-Justin, S,

728 Boulanger, P. (2017) High affinity anchoring of the decoration protein pb10 onto the
729 bacteriophage T5 capsid. Sci Rep 7: 41662.
730 42. Doore SM, Schrad JR, Dean WF, Dover JA, Parent KN (2018) Shigella Phages Isolated
731 during a Dysentery Outbreak Reveal Uncommon Structures and Broad Species
732 Diversity. J Virol 92.
733 43. Sathaliyawala T, Islam MZ, Li Q, Fokine A, Rossmann MG, Rao, VB. (2010) Functional
734 analysis of the highly antigenic outer capsid protein, Hoc, a virus decoration protein
735 from T4-like bacteriophages. Mol Microbiol 77: 444-455.
736 44. Fokine A, Islam MZ, Zhang Z, Bowman VD, Rao VB, Rossmann, MG. (2011) Structure
737 of the three N-terminal immunoglobulin domains of the highly immunogenic outer
738 capsid protein from a T4-like bacteriophage. J Virol 85: 8141-8148.
739 45. Choi KH, McPartland J, Kaganman I, Bowman VD, Rothman-Denes LB, Rossmann, MG.
740 (2008) Insight into DNA and protein transport in double-stranded DNA viruses: the
741 structure of bacteriophage N4. J Mol Biol 378: 726-736.
742 46. Wang Z, Hardies SC, Fokine A, Klose T, Jiang W, Cho, BC, Rossmann, MG. (2018)
743 Structure of the Marine Siphovirus TW1: Evolution of Capsid-Stabilizing Proteins and
744 Tail Spikes. Structure 26: 238-248 e233.
745 47. Qin L, Fokine A, O'Donnell E, Rao VB, Rossmann MG (2010) Structure of the small
746 outer capsid protein, Soc: a clamp for stabilizing capsids of T4-like phages. J Mol
747 Biol 395: 728-741.
748 48. Stone NP, Hilbert BJ, Hidalgo D, Halloran KT, Lee J, Sontheimer, EJ, Kelch, BA. (2018)
749 A Hyperthermophilic Phage Decoration Protein Suggests Common Evolutionary
750 Origin with Herpesvirus Triplex Proteins and an Anti-CRISPR Protein. Structure 26:
751 936-947 e933.
752 49. Shivachandra SB, Rao M, Janosi L, Sathaliyawala T, Matyas GR, Alving, CR, Leppla,
753 SH, Rao, VB. (2006) In vitro binding of anthrax protective antigen on bacteriophage
754 T4 capsid surface through Hoc-capsid interactions: a strategy for efficient display of
755 large full-length proteins. Virology 345: 190-198.
756 50. Yang F, Forrer P, Dauter Z, Conway JF, Cheng N, Cerritelli, ME, Steven, AC, Pluckthun,
757 A, Wlodawer, A. (2000) Novel fold and capsid-binding properties of the lambda-
758 phage display platform protein gpD. Nat Struct Biol 7: 230-237.
759 51. Forrer P, Chang C, Ott D, Wlodawer A, Pluckthun A (2004) Kinetic stability and crystal
760 structure of the viral capsid protein SHP. J Mol Biol 344: 179-193.
761 52. D'Lima NG, Teschke CM (2015) A Molecular Staple: D-Loops in the I Domain of
762 Bacteriophage P22 Coat Protein Make Important Intercapsomer Contacts Required
763 for Procapsid Assembly. J Virol 89: 10569-10579.
764 53. Baker TS, Olson NH, Fuller SD (1999) Adding the third dimension to virus life cycles:
765 three-dimensional reconstruction of icosahedral viruses from cryo-electron
766 micrographs. [erratum appears in Microbiol Mol Biol Rev 2000 Mar;64(1):237.].
767 Microbiology & Molecular Biology Reviews 63: 862-922.
768 54. Mastronarde DN (2005) Automated electron microscope tomography using robust
769 prediction of specimen movements. J Struct Biol 1: 36-51.
770 55. Wang Z, Hryc C, Bammes B, Afonine PV, Jakana J, Chen, DH, Liu, J, Baker, ML, Kao,
771 C, Ludtke, SJ, Schmid, MF, Adams, PD, Chiu, W. (2014) An atomic model of brome
772 mosaic virus using direct electron detection and real-space optimization. Nature
773 Communications 5: 4808.
774 56. Yan X, Dryden KA, Tang J, Baker TS (2007) Ab initio random model method facilitates
775 3D reconstruction of icosahedral particles. J Struct Biol 157: 211-225.
776 57. Yan X, Sinkovits RS, Baker TS (2007) AUTO3DEM-an automated and high throughput
777 program for image reconstruction of icosahedral particles. J Struct Biol 157: 73-82.

58. Bowman VD, Chase ES, Franz AW, Chipman PR, Zhang X, Perry, KL, Baker, TS, Smith, TJ. (2002) An antibody to the putative aphid recognition site on cucumber mosaic virus recognizes pentons but not hexons. J Virol 76: 12250-12258.
59. Pintilie G, Chen DH, Haase-Pettingell CA, King JA, Chiu W (2016) Resolution and Probabilistic Models of Components in CryoEM Maps of Mature P22 Bacteriophage. Biophys J 110: 827-839.
60. Goddard TD, Huang CC, Ferrin TE (2007) Visualizing density maps with UCSF Chimera. J Struct Biol 157: 281-287.
61. Altschul SF, Madden TL, Schaffer AA, Zhang J, Zhang Z, Miller, E, Lipman, DI. (1997) Gapped BLAST and PSI-BLAST: a new generation of protein database search programs. Nucleic Acids Res 25: 3389-3402.
62. Wu X, Brooks B (2007) Modeling Of Macromolecular Assemblies with Map Objects. BioComp 411-420.
63. Brooks BR, Brooks CL, 3rd, Mackerell AD, Jr., Nilsson L, Petrella RJ, Roux, B, Won, Y, Archontis, G, Bartels, C, Boresch, C, Caflish, A., Caevs, L, Cui, Q, Dinner, AR, Feig, M, Fischer, S, Gao, J, Hodoscek, M, Im, W, Kuczera, K, Lazaridis, T, Ma, J, Ovchinnikov, V, Paci, E, Pastor, RW, Post, CB, Pu, JZ, Schafer, M, Tidor, B, Venable, RM, Woodcock, HL, Wu, X, Yang, W, York, DM, Karplus, M (2009) CHARMM: the biomolecular simulation program. J Comput Chem 30: 1545-1614.
64. Granell M, Namura M, Alvira S, Kanamaru S, van Raaij MJ (2017) Crystal Structure of the Carboxy-Terminal Region of the Bacteriophage T4 Proximal Long Tail Fiber Protein Gp34. Viruses 9.
65. Trabuco LG, Villa E, Mitra K, Frank J, Schulten K (2008) Flexible fitting of atomic structures into electron microscopy maps using molecular dynamics. Structure 16: 673-683.
66. Phillips JC, Braun R, Wang W, Gumbart J, Tajkhorshid E, Villa, E, Chipot, C, Skeel, RD, Kale, L, Schulten, K. (2005) Scalable molecular dynamics with NAMD. J Comput Chem 26: 1781-1802.
67. Humphrey W, Dalke A, Schulten K (1996) VMD: visual molecular dynamics. J Mol Graph 14: 33-38, 27-38.
68. Cordier F, Grzesiek S (1999) Direct observation of hydrogen bonds in proteins by interresidue 3HJNC' scalar couplings. J Am Chem Soc 121: 1601-1602.
69. Lipari G, Szabo, A. (1982) Model-Free Approach to the Interpretation of Nuclear Magnetic Resonance Relaxation in Macromolecules. 1. Theory and Validity. J Am Chem Soc 104: 4546-4559.
70. Dosset P, Hus JC, Blackledge M, Marion D (2000) Efficient analysis of macromolecular rotational diffusion from heteronuclear relaxation data. J Biomol NMR 16: 23-28.
71. Henderson R, Sali A, Baker ML, Carragher B, Devkota B, Downing, KH, Egelman EH, Feng, Z, Frank, J, Grigorieff, N, Jiang, W, Ludtke, SJ, Medalia, O, Penczek, PA, Rosenthal, PB, Rossmann, MG, Schmid, MF, Schroeder, GF, Steven, AC, Stokes, DL, Westbrook, JD, Wriggers, W, Yang, H, Young, J, Berman, HM, Chiu, W, Kleywegt, GJ, Lawson, CL. (2012) Outcome of the first electron microscopy validation task force meeting. Structure 20: 205-214.
72. Kumar GS, Clarkson MW, Kunze MBA, Granata D, Wand AJ, Lindorff-Larsen, K, Page, R, Peti, W. (2018) Dynamic activation and regulation of the mitogen-activated protein kinase p38. Proc Natl Acad Sci U S A 115: 4655-4660.

827 **TABLES AND FIGURE LEGENDS**

828 **Tables:**

829 **Table 1. Statistics for the top 20 NMR structures of Dec.**
830

Experimental Restraints		
Total number of NMR restraints	1,009	
Total number of NOE distance restraints	767	
Ambiguous	73	
Unambiguous	694	
Long range (|i-j|>4)	124	
Medium range (|i-j|)≤4)	93	
Sequential (|i-j|)=1)	281	
Intra-residue NOEs	269	
Total number of dihedral restraints	174	
φ/ ψ	127	
χ_1	47	
Hydrogen bond restraints (34*2)	68	
RMSD from experimental restraints[a]		
NOE distance (Å)	0.054 ± 0.003	
Dihedral (°)	0.42 ± 0.14	
RMSD from ideal geometry		
Bonds (Å)	0.0042 ± 0.0001	
Angles (°)	0.55 ± 0.02	
Improper angles (°)	1.68 ± 0.12	
E_{L-J} (kcal/mol)	- 316 ± 44	
RMSD from mean NMR structure	Backbone [b]	All Heavy Atoms
Entire protein 1-134 (Å)	> 9.5	> 9.5
Folded regions 12-86 (Å)	1.33 ± 0.21	1.95 ± 0.32
OB-fold 18-77 (Å)	1.08 ± 0.18	1.66 ± 0.25
OB-fold 2° structure[c] (Å)	0.84 ± 0.15	1.57 ± 0.31
Procheck Ramachandran Plot Statistics[d]		
Most favored (%)	89.1	
Additionally allowed (%)	10.9	
Generously allowed (%)	0.0	
Disallowed (%)	0.0	
Quality Z Scores from PSVS[e]		
Procheck (□□□)	-2.64	
Molprobity Clash	-1.19	

831
832 [a] Structures had no NOE violations > 0.5 Å nor dihedral violations > 5 degrees.
833 [b] Atoms: Cα, N, C, O
834 [c] Calculated over residues in the OB-fold portion: 21-32 (β1), 35-40 (β2), 47-50 (β3), 52-59
835 (α_{OB}), 63-68 (β4), 73-77 (β5), a total of 41 amino acids.
836 [d] Calculated with the PSVS server (http://psvs-1_5-dev.nesg.org) using only the folded parts of
837 Dec (residues 12-89).
838

839 **Figures and Legends:**

840

841 **Figure 1: Cryo-EM imaging and icosahedral image reconstruction of the mature phage**
842 **L capsid.** A) Image reconstruction of phage L overlaid with a black icosahedral cage. The
843 different symmetry axes marked. The capsid is shown in grey and Dec density is shown in
844 cyan. Enlarged view of a quasi-3-fold symmetry axis between hexons showing the B) coat
845 protein and C)Dec. Both panels B and C show the density fitted with homology models
846 optimized by molecular dynamics-based flexible fitting.

847

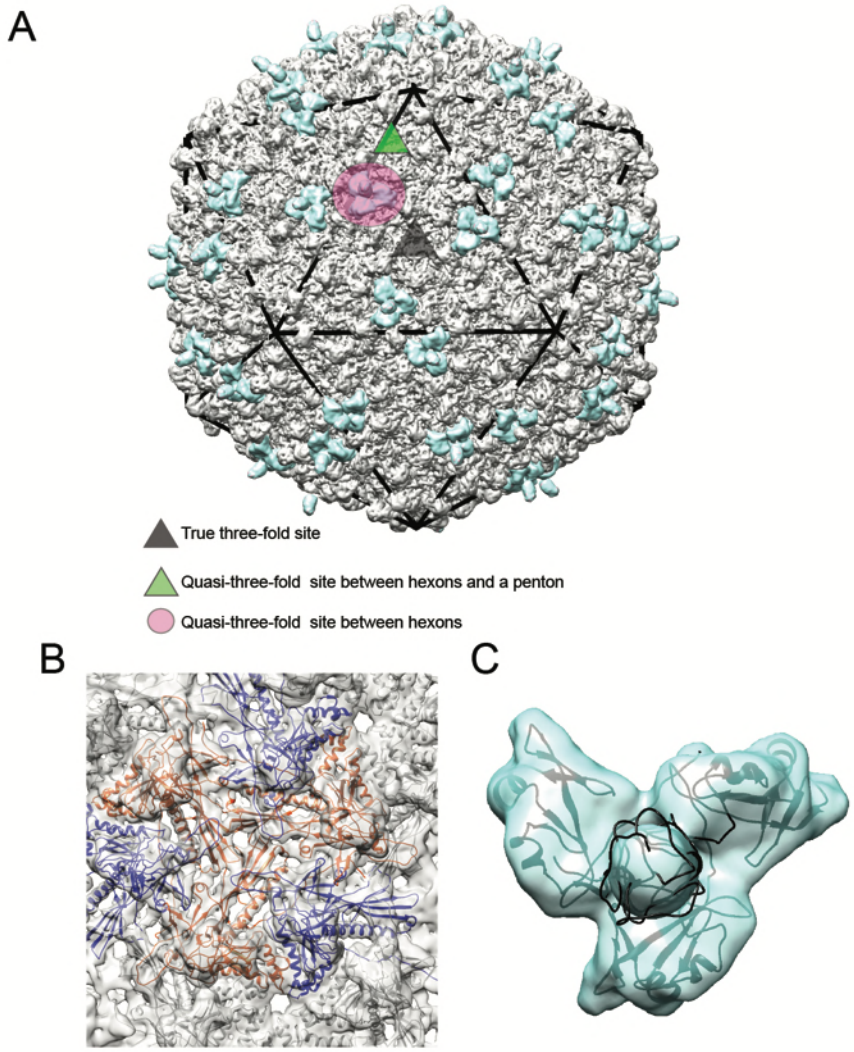

848

849 **Figure 2: NMR structure of the Dec monomer.** A) Ensemble of the 20 lowest-energy NMR
850 structures. For clarity, the disordered N- and C-termini are not shown. The folded globular
851 part of Dec has an OB-fold consisting of a β1-β3 meander (sky blue) and a β4-β5 hairpin
852 (yellow), with an α-helix (green) intervening between strands β3 and β4. Additional
853 secondary structure outside of the OB-fold incudes the short N-terminal strand β0 (dark
854 blue), and a C-terminal α-helix (pink). B) Cartoon showing the structure closest to the NMR
855 average. The first 10 N-terminal residues and the last ~45 C-terminal residues, which are
856 unstructured in the Dec monomers are colored red and orange, respectively. The coloring
857 scheme for the rest of the protein in this and subsequent panels is the same as in A. C)
858 Diagram summarizing the topology and secondary structure limits of the Dec monomers.

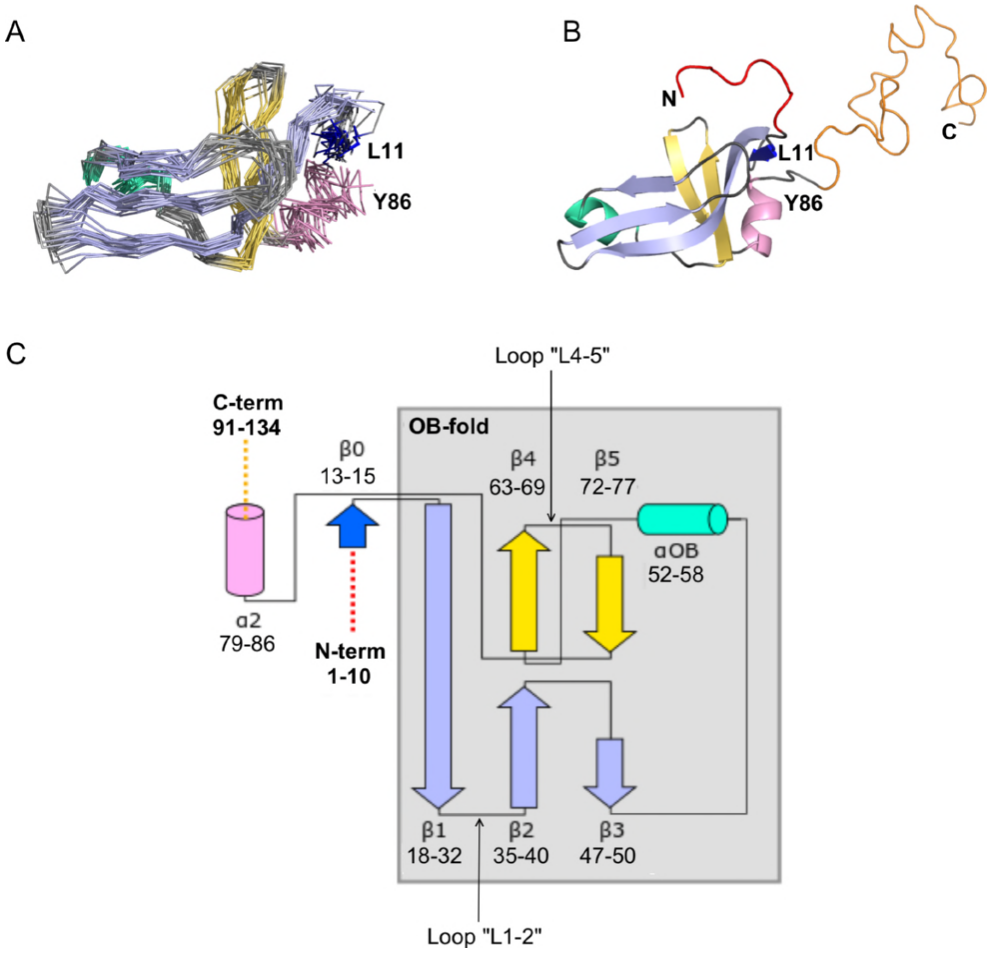

859

860

Figure 3: Comparison of cryo-EM and NMR structures. Superposition of the NMR Dec monomer structures onto the cryo-EM Dec trimer structure (maroon). The Dec monomer structures are colored as in Fig. 3.

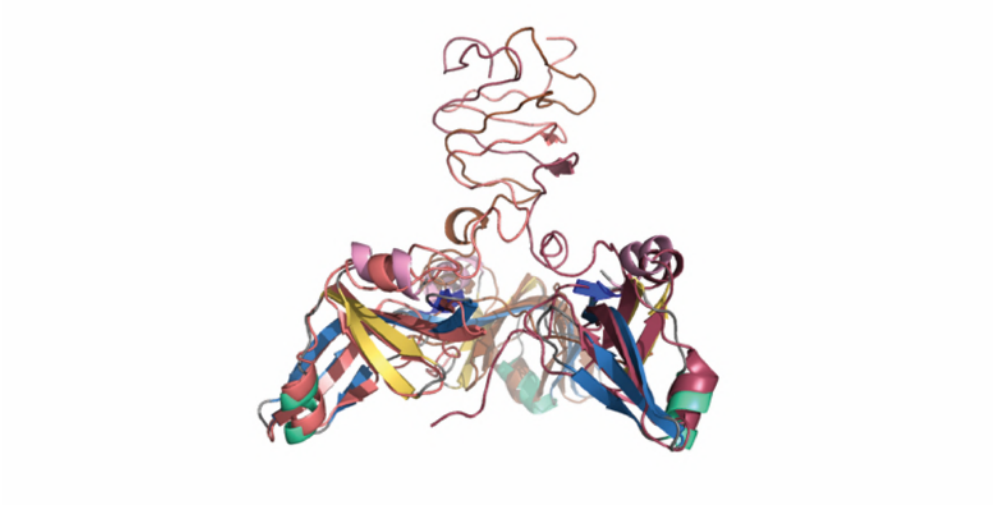

866 **Figure 4: Dynamics of the Dec monomer.** A) S^2 order parameters describing the
867 amplitude of fast motions on the ps-ns timescale. Rigid (S^2 > 0.65), moderately flexible (0.65
868 ≥ S^2 > 0.55), and highly flexible (0.55 ≥ S^2) sites are indicated by black, purple, and red
869 symbols respectively. The secondary structure of Dec is given at the top of panel A. B)
870 Contributions to R2 relaxation from slow conformational exchange on the µs-ms timescale.
871 Amide protons with moderate $R2_{ex}$ values smaller than 3 Hz are shown in purple, those with
872 large contributions above 3 Hz in red. The S^2 and $R2_{ex}$ parameters were obtained from a
873 Model-Free analysis [69] of ^{15}N R1, R2, and ^{1}H-^{15}N NOE relaxation data for Dec (Figure S4)
874 using the program TENSOR 2.0 [70]. In C) and D) the S^2 and $R2_{ex}$ values are mapped onto
875 the NMR structure ensembles for Dec. Residues 1-10 and 90-134 which are unfolded and
876 thus have the lowest S^2 values, are not shown in the structures
877

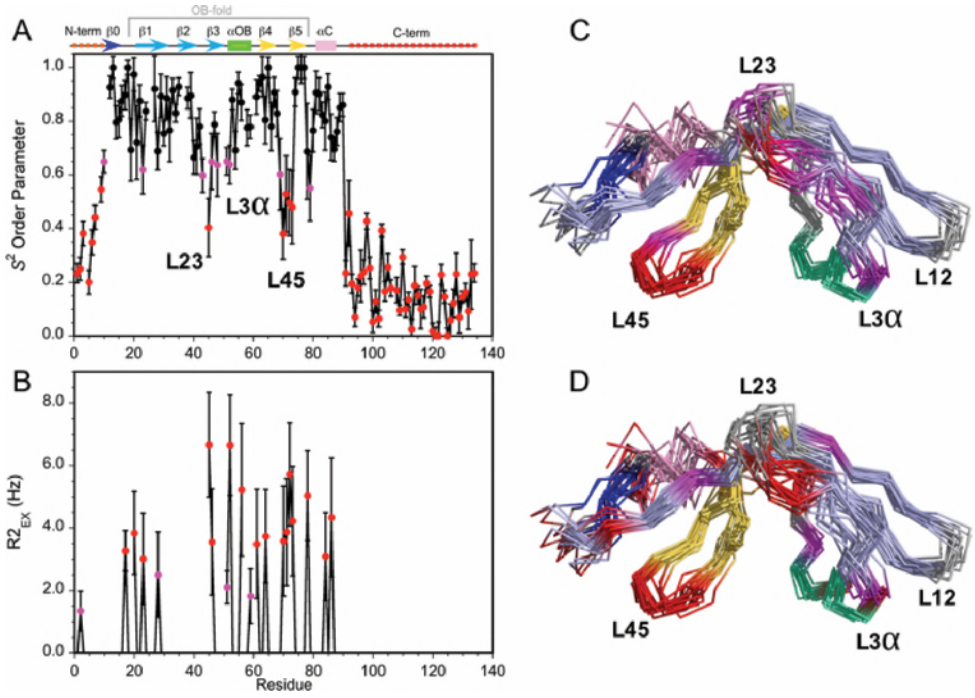

878
879

880 **Figure 5: Binding assays of variant coat proteins and Dec to probe the binding**
881 **interface.** A) Coat protein subunits depicted as ribbon diagrams around a quasi-3-fold axis
882 Dec binding site. Three coat subunits directly surrounding a quasi-3-fold axis are shown in
883 light grey, and three coat proteins occupying a neighboring quasi-equivalent conformation in
884 the lattice shown in black. Residues selected for mutagenesis are shown as spheres. B)
885 Normalized binding data of the ratio of variant coat protein bound to WT Dec, color-coded to
886 match the corresponding residues in panel A. C) Dec trimer shown as ribbons, with each
887 monomer a different shade of blue. Residues selected for mutagenesis are shown as
888 spheres. D) Enlarged view of the Dec cryo-EM density with a monomer shown as a ribbon.
889 K30 and Y49 residues are shown as spheres and the two different capsid binding sites are
890 circled. E) Normalized binding data of the ratio of WT coat protein bound to variant Dec, and
891 color-coded to match the corresponding residues in panels C and D.

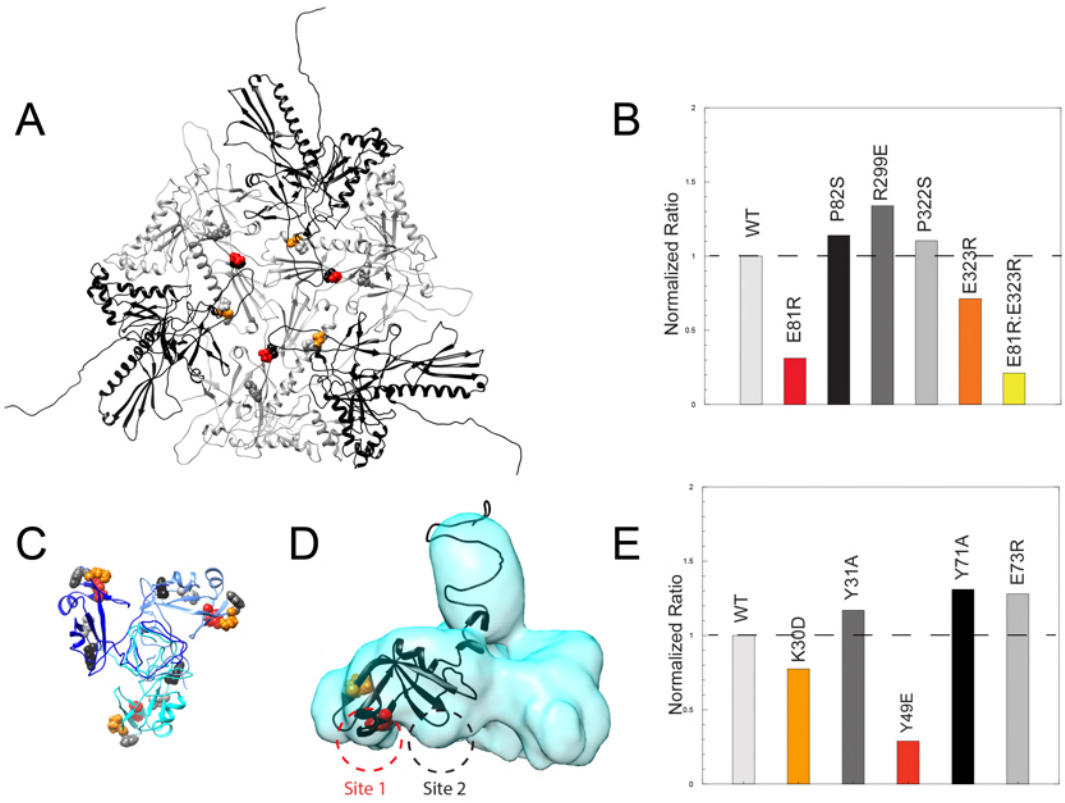

892

Figure 6: Dec demonstrates discriminatory binding at different types of three-fold symmetry axes. Dec trimer (red/pink) with surrounding capsid proteins (blue/ice blue). Darker colors show the Dec trimer at a quasi three-fold symmetry axis, lighter colors show the Dec trimer at the true three-fold axis. A and B show side and top views of a local region of each Dec-capsid complex. The close-ups C and D show the interface between Dec and one of the capsid proteins. Both complexes (Dec plus capsid) were superimposed using only the Dec coordinates for residues 10-88.

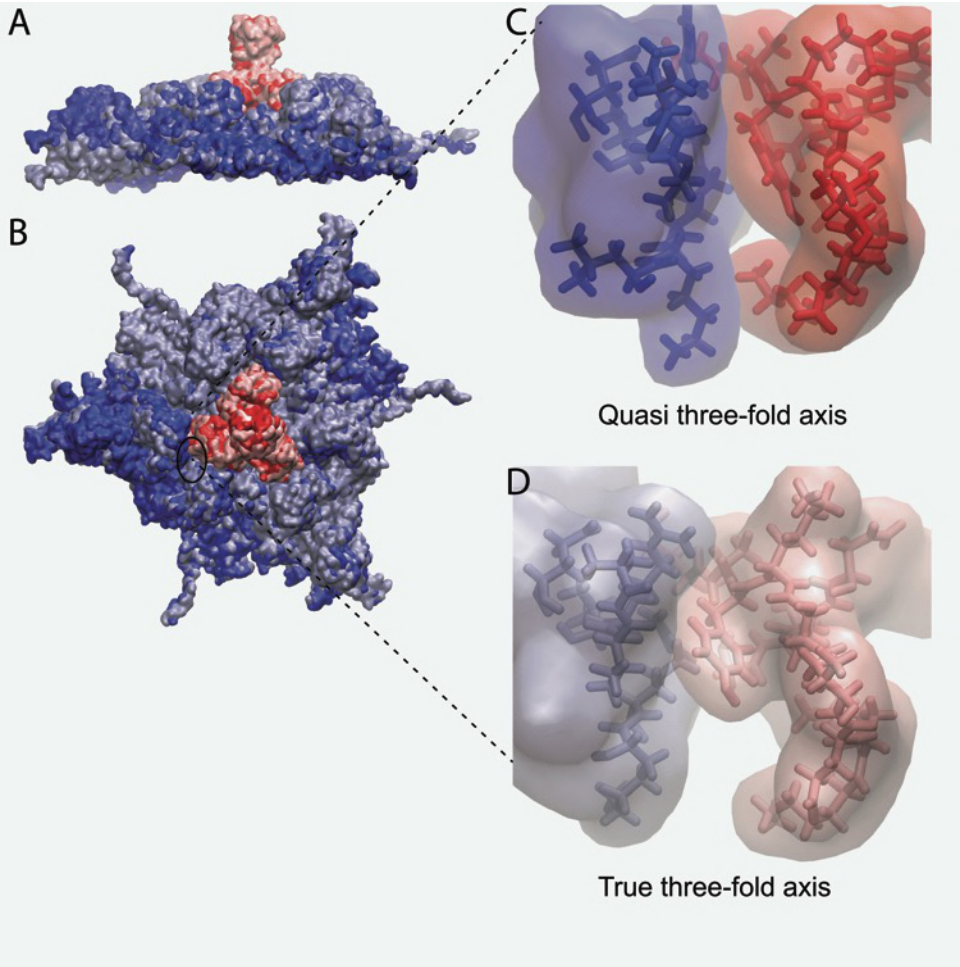

904 **Figure 7: Comparison of decoration proteins.** A) Side and B) top-down views of
905 decoration proteins gpD (PDB ID 1C5E), gp87 (PDB ID 6BL5) and Dec (PDB ID 6D2D).
906 Chains of each trimer are rainbow colored from N-terminus (blue) to C-terminus (red).
907

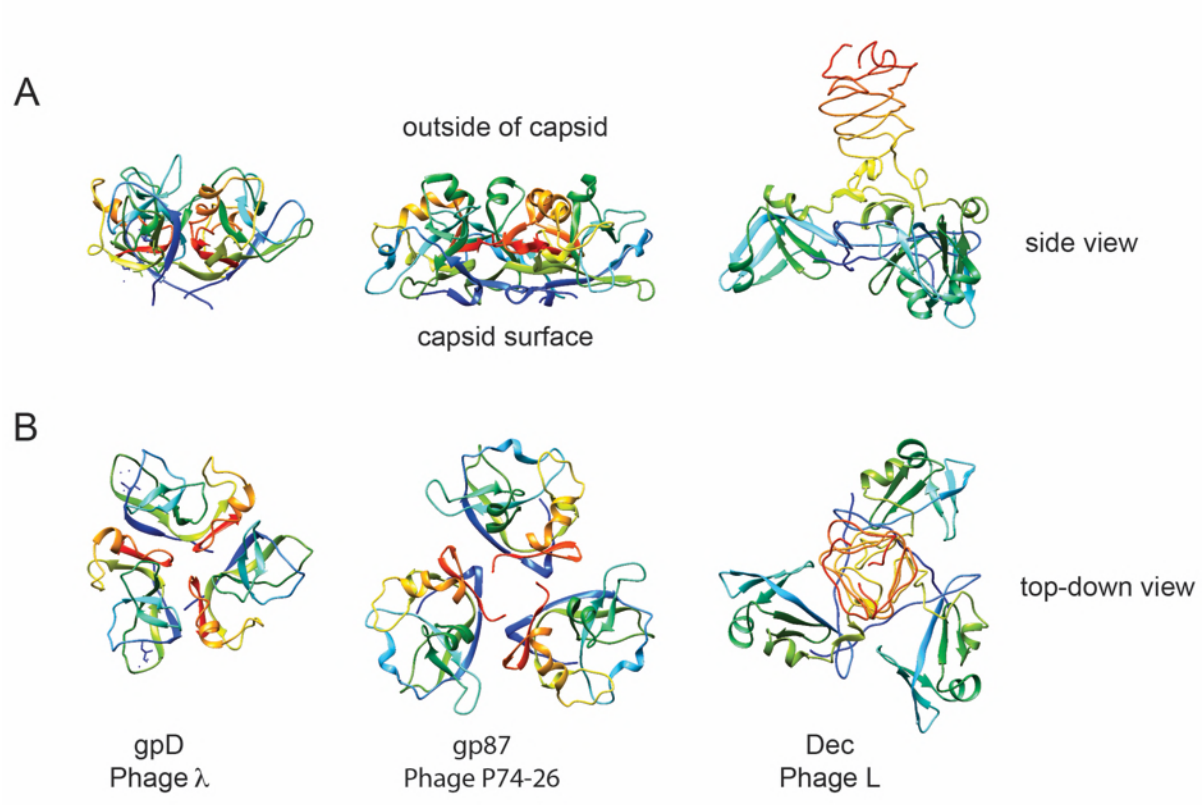

908
909
910 **Supplementary Figures/Tables/Movies Legends:**
911
912 **Table S1: Comparison of individual asymmetric units of the coat lattice with average**
913 **asymmetric unit and P22 structure**
914 We generated models for nine complete asymmetric units in order to completely fill the cryo-
915 EM density of one eighth of the total capsid (Figure S2 A-C). Figure S2 indicates where
916 each of these asymmetric units are located and corresponds to the data in Table S1. We

917 carried out the same analysis with respect to the P22 structure based on the PDB structure
918 (5UU5).
919
920 **Table S2: Comparison of individual Dec trimers with average structure**
921
922
923 **Figure S1): Phage L cryo-EM and 3D reconstruction data.** A) Representative micrograph
924 of frozen hydrated phage L particles. B) FSC curve with $FSC_{0.143}$ cutoff shown with a dashed
925 line. The red arrow points out the estimated global resolution of the map at 4.2 Å according
926 to the "gold standard" method [71].
927
928 **Figure S2): Phage L coat protein subunit and asymmetric unit.** We generated models
929 for nine complete asymmetric units in order to completely fill the cryo-EM density of one
930 eighth of the total capsid (Figure S2 A-C, Table S1). We carried out the same analysis with
931 respect to the P22 structure based on the P22 PDB structure (5UU5). The average phage L
932 structure deviates from the P22 structure (PDB 5UU5) by about 1 Å for the hexamer and 1.5
933 Å for the penton unit, which is in the range of what may be expected for structures of
934 homologous proteins [28]. A) Full phage L capsid shown in blue, with the octant of the map
935 used for modeling highlighted. Coat protein segmentation is colored in grey and the Dec
936 segmentation is colored in cyan. Note the map is rotated to peer down a true 3-fold axis in
937 the center of the area that was modeled. B) Protein subunits modeled using molecular
938 dynamics flexible fitting are shown as black ribbon diagrams and extend beyond the cryo-
939 EM density map edges. C) Coat protein asymmetric units (P0X) and Dec trimers (D0X)
940 labeled as listed in Tables S1 & S2. D) Single coat protein monomer shown color-coded
941 according to domain boundaries (N-arm in red, P-domain in green, E-loop in yellow, A-
942 domain in cyan, and I-domain in magenta). E) An asymmetric unit of coat proteins (PDB ID

943 6D2F), with six subunits from a hexon (A-F; red, orange, yellow, green, blue, and purple)
944 and one subunit from a penton (subunit G, black).
945
946 **Figure S3): Resolution of the phage L map is not uniform.** A) Phage L surface rendered
947 view, colored accorded to local resolution with an octant of the virion removed to show the
948 internal genome organization. The color bar indicates resolution in Å.
949
950 **Figure S4. Dec trimers structures have a flexible C terminus**; Dec trimer from a top-
951 down view (left) and rotated to a side view (right). Individual strands are colored yellow,
952 green, or rainbow colored to highlight the OB fold. In the N-terminal OB fold region, the
953 resolution of the map is much higher (ranges 3.8 – 4.5 Å) than the β–helix. We were able to
954 reliably fit side chains into the majority of the N-terminal density envelope (residues 10-88).
955 The average R2 and R1 values for the folded portions of Dec are about 13 Hz (Figure S5A)
956 and 1.4 Hz (Figure S5B), respectively. For comparison, a Dec trimer with a MW of 43 KDa is
957 expected to have R2 and R1 values near 50 Hz and 0.4 Hz, respectively [72]. Thus the ^{15}N
958 relaxation data for Dec samples subjected to our unfolding/refolding protocol are more
959 consistent with a 14.4 KDa Dec monomer than a trimer. Similarly, the Model Free analysis of
960 the ^{15}N relaxation data gives an optimum global correlation time for isotropic rotational
961 diffusion of 7.4 ns, consistent with a Dec monomer. For a 43 KDa trimer the value of the
962 correlation time should be about 21 ns.
963
964 **Figure S5. CS-ROSETTA modeling of the Dec monomer structure. (A)** The lowest
965 energy model based on the assigned NMR chemical shifts of Dec [30] has an OB-fold
966 topology. Only residues 10-88 were included in the CS-ROSETTA simulations [32], since
967 the program predicted that residues 1-9 and 89-134 are disordered, based on the assigned
968 NMR chemical shifts. The 5-stranded, Greek Key β-barrel OB-fold motif [24] is formed from

969 a β1-b3 meander (light blue) and a β4-β5 hairpin (yellow), with an α-helix (green) intervening
970 between strands β3 and β4. **(B)** Graph showing convergence of the CS-ROSETTA
971 simulations. The statistics indicated that the CS-ROSETTA simulations did not fully
972 converge. In spite of this, nine of the top ten lowest energy structures had an OB-fold
973 structure with an average RMSD of 2.5 Å to the structure shown in (A).
974
975 **Figure S6. ^{15}N relaxation values for monomeric Dec.** (A) R1, (B) R2, (C) ^{1}H-^{15}N NOE. All
976 data were recorded at 800 MHz, with a sample temperature of 33 ^{o}C. The secondary
977 structure of Dec, derived from its NMR structure, is indicated at the top of the first panel.
978
979
980 **Supplementary Movies**
981
982 **Movie S1**
983 Comparison of cryo-EM Dec trimer (grey) overlaid with the top ensemble structures from
984 NMR.
985
986 **Movie S2**
987 View of the segmentation and fitting process for a quasi-three fold axis of the phage L map.
988 Segmented Dec density is shown in cyan and the segmented coat protein density is shown
989 in grey. The Dec trimer backbone is shown as a ribbon diagram with each strand a different
990 shade of blue. The coat protein backbone lattice is shown as a ribbon diagram with the three
991 subunits directly surrounding the quasi-three-fold symmetry axis in grey. The three subunits
992 in black occupy a different position in the quasi-equivalent lattice, but overlap with the grey
993 subunits and contribute to the Dec binding site.
994

Movie S3. Key residues that modulate Dec binding affinity. View of the binding interactions between Dec and coat protein at a quasi-three-fold symmetry axis. Coat protein and Dec monomers are color coded as in Movie S2. Amino acid sites that were chosen for mutagenesis are shown as spheres and are color coded to match the data in Figure 6 of the main text.

Movie S4. Movie. S4 Definition of different regions of the Dec monomer NMR structure. To illustrate the precision of the structure all 20 members of the NMR ensemble are shown. The movie than flips through the 20 individual NMR structures to show the differences in precision between the structured OB-fold component, and the unstructured N- (yellow) and C-termini (orange). In the second half of the movie, the N- and C-termini are not shown to better illustrate differences in structural definition of the OB-fold component.